Available online at www.sciencedirect.com
ScienceDirect
Green Energy & Environment xxx (xxxx) xxx
www.keaipublishing.com/gee

Research paper

Computational screening and design of nanoporous membranes for efficient carbon isotope separation☆

Jingqi Wang [a], Musen Zhou [b], Diannan Lu [a,*], Weiyang Fei [a], Jianzhong Wu [b,*]

[a] Department of Chemical Engineering, Tsinghua University, Beijing, 100084, China
[b] Department of Chemical and Environmental Engineering, University of California, Riverside, CA, 92521, United States

Received 29 April 2020; revised 28 July 2020; accepted 29 July 2020
Available online ■ ■ ■

Abstract

Stable isotopes have been routinely used in chemical sciences, medical treatment and agricultural research. Conventional technologies to produce high-purity isotopes entail lengthy separation processes that often suffer from low selectivity and poor energy efficiency. Recent advances in nanoporous materials open up new opportunities for more efficient isotope enrichment and separation as the pore size and local chemical environment of such materials can be engineered with atomic precision. In this work, we demonstrate the unique capability of nanoporous membranes for the separation of stable carbon isotopes by computational screening a materials database consisting of 12,478 computation-ready, experimental metal-organic frameworks (MOFs). Nanoporous materials with the highest selectivity and membrane performance scores have been identified for separation of $^{12}CH_4/^{13}CH_4$ at the ambient condition (300 K). Analyzing the structural features and metal sites of the promising MOF candidates offers useful insights into membrane design to further improve the performance. An upper limit of the efficiency has been identified for the separation of $^{12}CH_4/^{13}CH_4$ with the existing MOFs and those variations by replacement of the metal sites.

Keywords: Metal-organic frameworks; Isotope separation; Computational materials design; Thermodynamics

1. Introduction

Stable isotope compounds are commonly utilized for both medical applications and scientific research [1–10]. For example, carbon-13 (^{13}C) have been broadly used in agriculture, medicine, and chemistry for labeling chemical species in different reactions, for the diagnosis of human diseases, and for tracing agricultural emission and biogeochemical cycles. Due to the tiny abundance of many isotopes in nature, widespread applications of isotope labeling and other uses hinge on technological progress for more efficient enrichment and separation.

Isotope separation is challenging because chemical compounds of different isotopes have near identical physicochemical properties and molecular characteristics. Conventional techniques, such as thermal diffusion, the Girdler sulfide process, ionic liquid adsorption, and cryogenic distillation, require intensive energy input and excess operational and equipment cost due to the low separation efficiency [11–22]. Although the selectivity can be improved via laser activation, magnet fields and supersonic beams [23,24], the high cost limits their applications to small scale isotope productions [25,26]. To satisfy the increasing demand for isotope compounds, we need to develop low-cost and more energy-efficient separation processes suitable for mass production.

☆ The authors dedicate this work to Professor Wenchuan Wang, one of the pioneers applying molecular thermodynamics and Monet Carlo simulation to chemical engineering in China.

* Corresponding authors.
E-mail addresses: ludiannan@tsinghua.edu.cn (D. Lu), jwu@engr.ucr.edu (J. Wu).

https://doi.org/10.1016/j.gee.2020.07.025

Nanoporous materials are promising for separation of isotope compounds owing to their tunable pore sizes and chemical affinities. Recently, numerous studies have been reported on the applications of different kinds of nanoporous materials for gas storage and separation, such as activated carbons, zeolites, covalent-organic frameworks (COFs) and metal−organic frameworks (MOFs) [27–31]. In particular, MOFs are a class of crystalline materials consisting of metallic clusters and organic linkers [27,32–34]. The modular nature of the framework structure allows for the design and a precise control of the aperture size, binding sites, and mechanic strength by altering the topological structure and building blocks [8,35]. Tunable pore size and local chemical composition make MOFs excellent candidates for various applications such as CO_2 capture [34,36–39], drug delivery [40], isotopologue sieving [35,41,42] and chemical sensing [32,43].

MOFs have been previously investigated to separate isotope components [44]. They are particularly promising for H_2/D_2 separation owing to the kinetic and chemical-affinity quantum sieving effects. While kinetic quantum sieving distinguishes isotopic species by the pore size, chemical-affinity quantum sieving leverages the difference in the binding energies. In our previous work [7], we studied the potential of hypothetical MOFs for separating $^{12}CH_4/^{13}CH_4$ by considering their slight difference in adsorption isotherms. Whereas promising adsorbents can be identified by computational screening a large library of hypothetical MOFs, it remains questionable whether these materials can be experimentally synthesized for $^{12}CH_4/^{13}CH_4$ separation. Here we consider a new materials database that consists of 12,478 computation-ready, experimental MOFs (CoRE MOF 2019) for their possible use as adsorbent or membrane in separation of $^{12}CH_4$ and $^{13}CH_4$. The isotopic pairs of methane are widely distributed in nature and have relatively low molecular masses. As the difference between ^{12}C and ^{13}C is only by one neutron, the lower molecular mass, the more significant in the disparity of their physical properties. The performance of these nanoporous materials are evaluated over a broad range of conditions in terms of the adsorption amount and selectivity for adsorption processes, and in terms of permeability and selectivity for membrane separation. Promising MOF candidates have been identified for both adsorption and membrane separations. By analyzing the structural features and metal sites of the top-performance MOFs, we are able to gain insights for the design of nanoporous materials with further improvement of separation efficiency. The MOF metal sites can be modified by changing the salt precursor during the synthesis. To help the experimental design, we have explored possible improvements by substituting the original metal sites with new ones of different size and energy parameters. For the MOF with the highest membrane selectivity of $^{12}CH_4/^{13}CH_4$, we observe an upper limit of the membrane selectivity by modifying only the metal sites.

2. Computational methods

2.1. Molecular model

The intermolecular potential between the isotopic forms of methane, $^{12}CH_4$ and $^{13}CH_4$, are represented by the single-site Lennard-Jones (LJ) model. Their interactions with individual MOF atoms are described in terms of the LJ (12-6) potential. The Lorentz−Berthelot mixing rule is used to calculate the binary parameters for different species. For all atoms from the MOF materials, the force field parameters are obtained from the universal force field (UFF) [45]. Like our previous work [8], the LJ parameters for $^{12}CH_4$ and $^{13}CH_4$ are calculated from the experimental data for the saturated vapor pressure at different temperatures according to the principle of corresponding state [46–48]. These parameters are listed in Table S1 [49]. A cutoff of 12.9 Å is applied to the calculation of all intermolecular interactions.

2.2. Ideal adsorption selectivity

We use the ideal adsorbed solution theory (IAST) [50] to assess the performance of different MOFs for separation of $^{12}CH_4$ and $^{13}CH_4$ by adsorption. At a given temperature, the ideal adsorption selectivity is defined by the ratio of Henry's constants:

$$\alpha^{IM} = K_{h,2}/K_{h,1} \tag{1}$$

where superscript *IM* represents an ideal mixture, i.e., the adsorption of methane at low pressure such that the interaction between gas molecules is negligible. Henry's constant is determined from the overall energy of a gas molecule interacting with the porous material, $V_{ext}(\mathbf{r})$,

$$K_h = \frac{1}{\Omega}\int d\mathbf{r}\,\exp\left[-\frac{V_{ext}(\mathbf{r})}{k_B T}\right] \tag{2}$$

where Ω represents the system volume, and k_B is the Boltzmann constant. For an ideal gas, the adsorption amount per unit volume of the adsorbent is proportional to pressure and Henry's constant.

2.3. Ideal membrane selectivity

In Henry's region (viz., at low gas pressure), the membrane selectivity can be written as the ratio of Henry's constants multiplied by the ratio of the diffusivity coefficients at infinite dilution [51,52]:

$$k^{IM} = \frac{K_{h,2}}{K_{h,1}}\frac{D_{0,2}}{D_{0,1}} = \frac{P_2}{P_1}. \tag{3}$$

here permeability P equals to the product of Henry's constant, K_h, and self-diffusion coefficient at infinite dilution, D_0 [52].

Unlike adsorption selectivity, membrane selectivity depends on both the equilibrium and transport properties of individual compounds. The latter can be predicted from the transition-state theory (TST). At infinite dilution, the diffusion coefficient for gas molecules in a porous material can be estimated from molecular hopping between neighboring cages:

$$D_0 = \frac{1}{2}\varpi a^2 \tag{4}$$

where a stands for the distance between a gas molecule in the initial and final states of hopping (i.e., between the positions of minimum energy states in two neighboring cages), and ϖ represents the transmission frequency or the hopping rate. The latter is calculated from

$$\varpi = \sqrt{\frac{k_B T}{2\pi m}} \frac{\exp[-V^{ext}(s^*)/k_B T]}{\int_0^1 \exp[-V^{ext}(s)/k_B T]ds} \tag{5}$$

where m stands for the molecular mass, s is defined as a normalized reaction coordinate or diffusion path ($0 \leq s \leq 1$) that connects the initial ($s = 0$) and final ($s = 1$) state of gas hopping, and the integral is carried over along the coordinate of gas hopping. The superscript * denotes the transition state of gas hopping between neighboring cages. Similar to our previous work, we use the string method [53,54] to determine the transition state and the minimum-energy diffusion pathway.

To establish a connection between materials chemistry and separation perfromance, we characterize the structural features of the promising MOFs such as the largest cavity diameter (LCD), the pore limiting diameter (PLD), the void fraction, void volume and specific surface area. We evaluate all these features using the Zeo++ [55] software in complement with UFF.

3. Results and discussion

3.1. Selectivity and capacity

In general, separation efficiency can be defined in terms of selectivity and capacity. For gas separation by pressure swing adsorption (PSA) or temperature swing adsorption (TSA) processes, the selectivity is defined by the relative amount of adsorption for different chemical species, and the capacity can be measured in terms of the total adsorption amount. For separation by permeation through a membrane, the selectivity depends on both the solubility/adsorption and diffusivity, and the capacity is defined by the permeability. In this work, we have considered the potential use of MOFs both as adsorbents and membranes for separation of the isotopic forms of methane.

The adsorption selectivity decreases exponentially with the increase of the adsorption amount (Fig. S1). As a result, the MOFs considered in this work have only limited applicability as the adsorbent for $^{12}CH_4$ and $^{13}CH_4$ separation. However, the membrane selectivity is less dependent on the separation capacity. As shown in Fig. 1, a good selectivity can be achieved by membrane separation at high permeability. Among 12,478 MOFs from the CoRE database, the material encoded "RUBLEH" exhibits both outstanding membrane selectivity and separation capacity. Its selectivity and permeability surpass the Robeson boundary, i.e., the upper limit of the correlation between selectivity and permeability for polymer membranes. Although most MOFs from the CoRE database have the selectivity and permeability values located underneath the Robeson boundary, we are able to identify a number of materials exceeding the Robeson boundary. In other words, these MOFs will have a better performance than the state-of-art polymer membranes for $^{12}CH_4/^{13}CH_4$ separation. As demonstrated in our previous work [8,9], MOF membranes can well balance the separation capacity and selectivity for isotope separation. However, their application as adsorbents is often compromised by the opposite trends in selectivity and capacity.

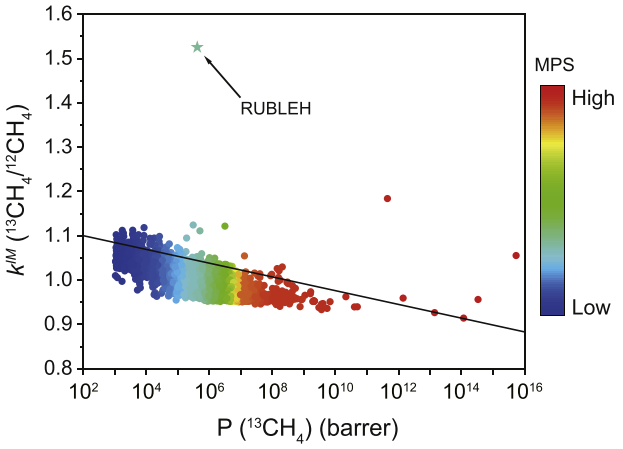

Fig. 1. Ideal membrane selectivity of 12,478 MOFs from the CoRE database versus the permeability of $^{13}CH_4$ at 300 K. Here the solid line represents the Robeson boundary, MPS stands for the membrane performance scores, and RUBLEH is the MOF with the highest selectivity.

Table S1 shows that $^{13}CH_4$ has a molecular diameter (viz., LJ size parameter) smaller than that of $^{12}CH_4$. However, its diffusivity in MOFs is not always larger than that of $^{12}CH_4$ as one would expect for bulk systems. The different trends reveal gas diffusion inside a nanoporous material depending not only on the molecular mass and size but also on the interaction of the gas molecule with the material, more specifically, on the diffusion path defined by the energy landscape. Table 1

Table 1
Permeability and membrane selectivity of top 5 MOFs for $^{12}CH_4/^{13}CH_4$ separation ranked according to the ideal membrane selectivity at 300 K.

MOF	Metal Site	P ($^{13}CH_4$) (barrer)	k^{IM}($^{13}CH_4/^{12}CH_4$)
RUBLEH	Zr	4.163×10^5	1.5255
YEGKIG	Zn	4.465×10^{11}	1.1839
MAGCEF	Zn	3.086×10^5	1.1242
HUWHOY	Cd	3.127×10^6	1.1216
GUNZIA	Cd	8.478×10^3	1.1184

summarizes the metal atoms, permeability, and membrane selectivity of top 5 MOFs ranked according to the ideal membrane selectivity. The crystal information (cif) files of these materials are provided in Supporting Information.

To understand why RUBLEH achieves such a high selectivity for $^{12}CH_4/^{13}CH_4$ separation, we present in Fig. 2 the energy profiles for their diffusion along the corresponding minimum-energy paths identified by the string method as well as the difference in energy along the diffusion coordinates. We observe significant difference in the energy profiles for the isotopic forms of methane near the transition states. Although RUBLEH contains zirconium metal sites with only a relatively weak LJ energy parameter, the material has micropores (LCD = 3.96 Å and PLD = 2.84 Å) comparable to the LJ diameters of the molecules. The significant difference in the energy profiles of $^{12}CH_4$ and $^{13}CH_4$ along the diffusion pathways lead to efficient sieving for separation of these two isotopic forms methane by RUBLEH.

To understand how $^{12}CH_4/^{13}CH_4$ separation keeps a good balance between high capacity and selectivity, we analyze the structural features of those promising MOF materials. Fig. 3 shows the distributions of LCD, PLD and void fraction for MOFs with top 5% membrane selectivity (k^{IM}). Clearly, the PLD of the top ranked MOFs is mostly distributed between 2 and 4 Å, or more precisely, from 2.6 Å to 3.3 Å. The narrow range of PLD indicates that small nanopores are beneficial to boost the membrane selectivity. The optimal pore size should be comparable with the LJ diameter of methane molecules, which is around 3.6 Å. It is evident that a careful construction of PLD around the molecular size is of central importance for membrane separation.

While PLD determines the energy barrier of molecular diffusion in a porous material, LCD is most closely related to the diffusion coordinate. Fig. 3a shows the distributions of MOFs with top 5% k^{IM} in term of PLD and LCD. Unlike PLD, the LCD values span in a wide range. While MOF with a small LCD provides a more confined space and thus better distinguishes methane molecules in different isotopic forms, a tight pore also hinders molecular hopping, leading to an unfavorable diffusion. As a result, most MOFs with top 5% k^{IM} have LCD in the range between 3 and 5 Å. We have also analyzed the interaction energy between MOF and the gas molecules (not shown) and found that MOFs with high membrane selectivity are correlated with a strong attraction along the diffusion path.

The void fraction of MOFs affects the permeability of gas molecules along with many other factors such as the types of lattice (e.g., fcc and simple cubic) and the membrane-penetrant interaction energies [56]. As shown in Fig. 3b, most MOFs with top 5% ideal membrane selectivity have an intermediate void fraction (~0.40). Materials with a small void fraction (viz. dense atomic packing) may lead to a low separation capacity but with high selectivity, while materials with a large void fraction would hardly be able to provide molecular-

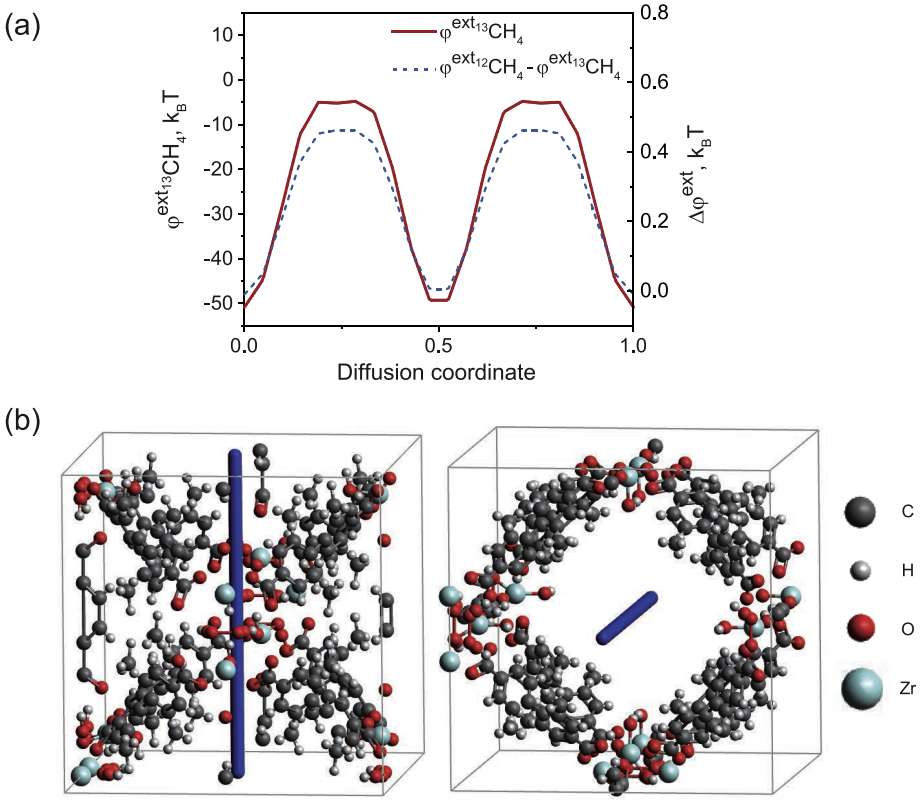

Fig. 2. (a) The energy landscape and (b) schematic of $^{13}CH_4$ minimum energy path for carbon isotope separation with RUBLEH membrane. The blue line stands for the minimum energy pathway of $^{13}CH_4$.

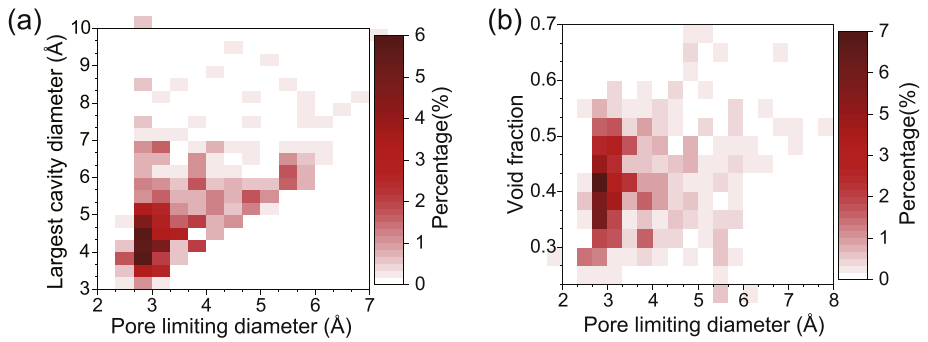

Fig. 3. Percentages of MOFs with top 5% ideal membrane selectivity in terms of PLD and LCD (a) and of PLD and the void fraction (b).

size confinement to sieve the gas molecules because the void fraction is correlated with PLD for reticular frameworks with the same topology (shown in Fig. S2).

A broad range of metal elements have been incorporated into MOFs, ranging from transition metal elements (e.g., Zn, Cd and Cu) to rare earth elements and alkali metal elements (e.g., Li, Na). To understand how the diverse metal elements affect the separation efficiency, we analyzed the percentage of metals in the CoRE database with top 5% ideal membrane selectivity for $^{12}CH_4/^{13}CH_4$ separation. Since most MOFs with top 5% k^{IM} have a PLD between 2 and 4 Å (shown in Fig. S3), we compare the percentage of metal sites with top 5% k^{IM} with that of MOFs with PLD in the range from 2 to 4 Å. By comparison of MOFs in the same range of pore size, we avoid sampling bias that would be introduced if the entire database is used.

Fig. 4a shows the percentages of metal elements of the most promising MOFs in comparison with those in the background. In our analysis, metal elements with the percentage smaller than 0.5% in the CoRE 2019 database are excluded because MOFs with metal sites in such a small percentage may indicate structural instability or limited experimental replicability [57]. Table S4 presents the percentages of metal elements in different categories according to membrane selectivity in details.

To better understand how the percentage of metals in top 5% k^{IM} is different from the background in comparison, we present in the inserted graph of Fig. 4a both the quotients and differences calculated by the percentage in top 5% k^{IM}. Here the quotient is defined as the percentage of metal site divided by that in the background, and the difference means the metal percentage subtracted by that in the background. The quotient is always larger than one, and the difference is always positive. Here metal sites with the highest quotient (Al), difference (Zn) and energy parameter (In) are marked with stars. According to the Lorentz–Berthelot mixing rule, the larger the energy parameter is, the more the adsorption energy would differ. Therefore, the top 3 metals with the highest quotients (Al, In and Ga) have the LJ energy parameters much higher than of methane, suggesting that metal elements with large energy parameters could significantly enhance the membrane selectivity. Half of the metals do not exhibit a noticeable difference because of their low percentage of presence in the CoRE database. For the top 3 metals with the largest difference in percentage (Zn, Al and In), they all have relatively large LJ energy parameters in comparison to other metals. However, not all of them have LJ energy parameters larger than those for the isotopic forms of methane.

Table 2 presents the LJ parameters for metal sites contained in the CoRE database. For most metals shown in Fig. 4a, the LJ energy parameters are not much higher than those for the two isotopic forms of methane. Fig. 4b and c display representative structures of MOFs containing metal sites with low (BOQYUD) and high (SOMFEG) energy parameters but with similar membrane selectivity. BOQYUD contains Fe (ε/k_B = 65.42 K) while SOMFEG contains In (ε/k_B = 301.43 K). In order to have similar membrane selectivity, BOQYUD (LCD = 3.38 Å and PLD = 2.82 Å) has a pore size much smaller than that for SOMFEG (LCD = 6.68 Å and PLD = 6.30 Å), indicating that, to achieve similar selectivity, a more confined structure is required for MOFs containing metal sites with a lower energy parameter.

3.2. Membrane performance score

For separating a pair of chemical species, the membrane performance score (MPS) is defined by the selectivity multiplied by the permeability:

$$MPS = S_{fast/slow} \times P_{fast} \quad (6)$$

where $S_{fast/slow}$ stands for the membrane selectivity of the fast diffusing species over the slow diffusing species, P_{fast} is the permeability of the fast specie. Similar to the adsorbent performance score (APS), MPS evaluates the overall membrane performance in separation processes because it takes into account both selectivity and capacity [9].

Table 3 lists the metal elements, $^{13}CH_4$ permeability, membrane selectivity, and MPS for top 5 MOFs with the highest MPS values. As shown in Fig. 1, MOFs with the highest MPS values have extremely high permeability but mediocre membrane selectivity for the separation of $^{12}CH_4/^{13}CH_4$. This suggests that, for $^{12}CH_4/^{13}CH_4$ separation at industrial scales, an extremely high membrane selectivity of MOFs does not compensate the loss of separation capacity compared to cases with intermediate membrane selectivity. It is also worth noting that the membrane selectivity of the top 5

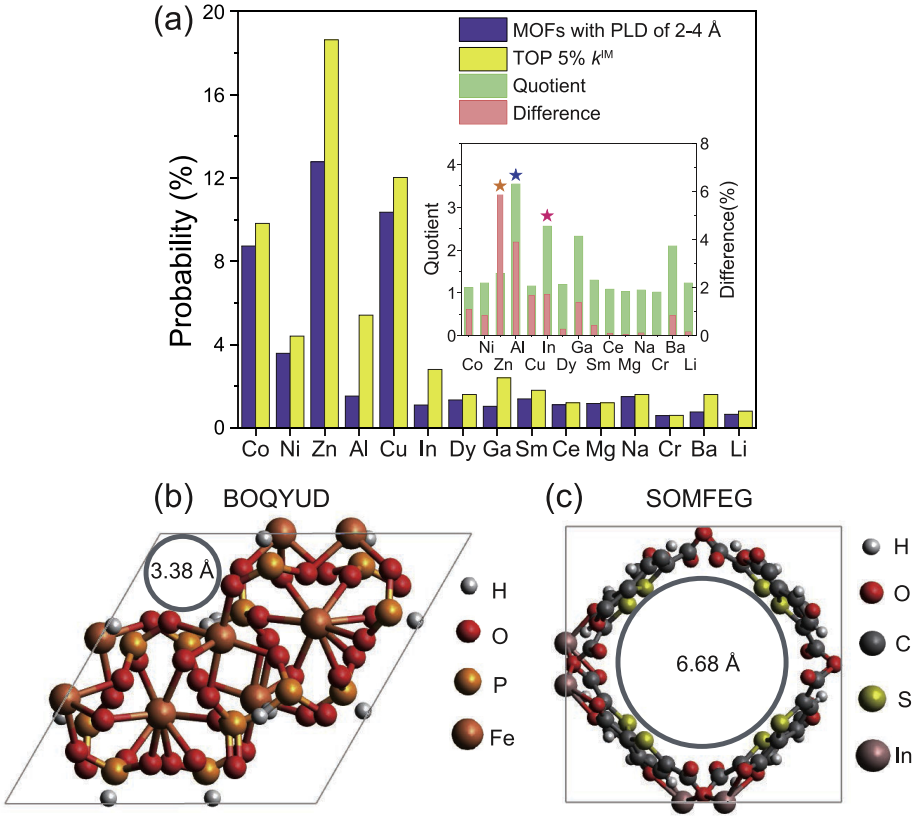

Fig. 4. (a) Percentages of the metal elements in the CoRE MOF database with top 5% ideal membrane selectivity and those MOFs with PLD in the range of 2–4 Å (background). Blue, orange and pink stars are used to denote the metal elements with the largest quotient, the largest difference, and the largest energy parameter. Atomistic structures and the largest cavity diameters of MOF (b) BOQYUD (k^{IM} = 1.0453) and (c) SOMFEG (k^{IM} = 1.0447).

MOFs ranked according to the membrane performance score is much lower than that of the top 5 MOFs ranked according to the membrane selectivity. Nevertheless, the membrane selectivity is still much higher than the selectivity achieved by best candidate from hypothetical MOF database via adsorption separation [7].

Fig. 5 and Fig. S6 present the correlation and distribution of structural features of MOFs with top 5% MPS values. In comparison with MOFs with top 5% k^{IM}, the PLD distribution is shifted toward a higher value (3–5 Å) in MOFs with top 5% MPS. Because MOFs with a high permeability are favored in MPS ranking, materials with high MPS offer a less confined structure. Similar to PLD, the distribution of LCD and void fraction for MOFs with top 5% MPS are also shifted toward larger values compared to those with top 5% k^{IM} in order to construct less confined MOF structures.

We have also analyzed the distributions of metal elements in MOFs with top 5% MPS. Fig. 6 shows the percentages of various metal elements in top 5% MPS in comparison with the background distributions. Similar to the analysis of metals in top 5% membrane selectivity, only metals with more than 0.5% in CoRE MOF 2019 database are considered and metals in MOFs with PLD between 3 and 6 Å are used for comparison in order to avoid sampling bias. Most MOFs with top 5% MPS have PLD at the same range (shown in Fig. S6 and Fig. S7). Detailed percentages of all metal elements in MOFs with top 5% MPS are listed in Table S5.

Similar to metals in MOFs with top 5% membrane selectivity, top 3 metal elements with highest quotient have

Table 2
The LJ parameters of metal elements. The force field parameters are from the universal force field (UFF) [45]. The italic font is used for metal elements overlapped in top 5% MPS and top 5% k^{IM}, and bold font is used for elements with energy parameter higher than that for methane.

Element	ε/k_B (K)	σ (Å)	Element	ε/k_B (K)	σ (Å)	Element	ε/k_B (K)	σ (Å)
Co	7.05	2.56	Ni	7.55	2.52	Zn	62.40	2.46
Dy	3.52	3.05	Sm	4.03	3.14	Na	15.10	2.66
Ce	6.54	3.17	Cr	7.55	2.69	Ba	183.17	3.30
Li	12.58	2.18	***Al***	***254.12***	***4.01***	*Cu*	*2.52*	*3.11*
Ga	***208.83***	***3.90***	*Mg*	*55.86*	*2.69*	***In***	***301.43***	***3.98***
Cd	114.73	2.54	Ca	119.77	3.03	**Si**	**202.29**	**3.83**
Y	36.23	2.98						

Table 3
Top 5 MOFs for the separation of $^{12}CH_4/^{13}CH_4$ according to the membrane performance score at 300 K.

MOF	Metal site	P ($^{13}CH_4$) (barrer)	k^{IM}($^{13}CH_4/^{12}CH_4$)	MPS
ERANAO	Zr	5.385×10^{15}	1.0553	5.683×10^{15}
XOPVOO	Ni	3.341×10^{14}	0.9561	3.655×10^{14}
OQIKOQ	Zr	1.166×10^{14}	0.9141	1.396×10^{14}
OJUNIS	Zn	1.399×10^{13}	0.9264	1.630×10^{13}
WOMFEK	Mn	1.406×10^{12}	0.9591	1.528×10^{12}

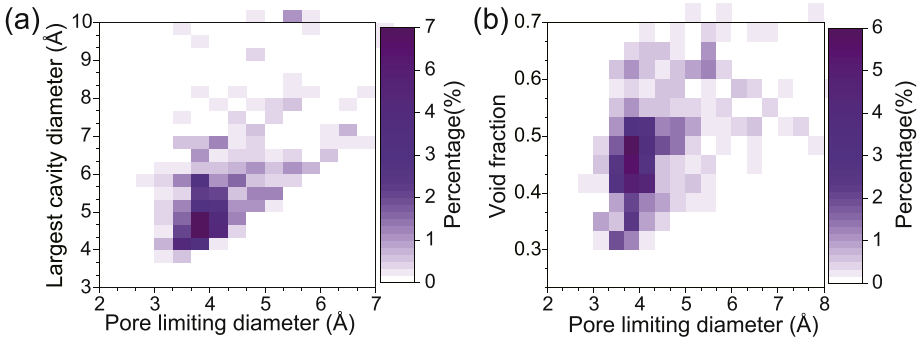

Fig. 5. Percentages of MOFs with top 5% MPS represented in terms of PLD and LCD (a) and in terms of PLD and the void fraction (b).

relatively large LJ energy parameters. In Table 2, the italic font is used for metal elements overlapped in top 5% MPS and top 5% k^{IM}, and bold font is used for elements with energy parameter higher than that for methane. Although metal elements in top 5% MPS are quite different from those in top 5% k^{IM}, a few of them (Al, Cu, Ga, Mg and In) are still overlapped, especially those with the LJ energy parameters larger than those corresponding to the two isotopic forms of methane. This indicates that metal elements in MOFs with large energy parameters are favored to achieve both high membrane selectivity and membrane performance score.

3.3. Modification of metal sites in MOFs

As discussed above, metal elements play an important role in the MOF performance for $^{12}CH_4/^{13}CH_4$ separation. In experiments, metal sites can be alternated by changing the salt precursor without altering the MOF topology. Therefore, in this section, we investigate how changes in the metal sites would influence the MOF performance for $^{12}CH_4/^{13}CH_4$ separation in terms of the membrane selectivity and MPS. Metal sites in top 5 MOFs with the highest membrane selectivity and the highest MPS are substituted with metal elements that are promising to further improve their performance.

For top 5 MOFs with the highest membrane selectivity, aluminum and zinc are used to substitute the original metal sites because their percentages in MOFs with top 5% k^{IM} are very different from those in the background in terms of both quotient and difference. In addition, indium is also selected to substitute the metal sites in top 5 MOFs with highest k^{IM} because it has the largest LJ energy parameter. Considering the small difference in the van der Waals interaction of MOFs with $^{12}CH_4$ and $^{13}CH_4$ molecules, we hypothesize that the larger the energy parameter of the metal is, the more differences in the binding energy of the MOF with $^{12}CH_4$ and $^{13}CH_4$. Intuitively, the trend can be understood from the Lorentz–Berthelot mixing rule.

Table S6 compares the performance (viz. permeability and membrane selectivity) of top 5 MOFs with the highest k^{IM} before and after substitution of the metal sites. Interestingly, the permeability of both $^{12}CH_4$ and $^{13}CH_4$ increases with the energy parameter for the metal site for all top 5 MOFs, while the trend for the membrane selectivity is totally opposite. To understand the different trends, we further substitute the metal site in RUBLEH (highest k^{IM}) with those metal elements shown in Fig. 4a.

As shown in Fig. 7a, the membrane selectivity exhibits an almost linear relation with the LJ energy parameter of the metal elements. We can improve the membrane selectivity up to 1.530 for RUBLEH by substituting Zr (original element for the metal sites) with Cu. Fig. 7b and c show the minimum energy along the diffusion coordinate for RUBLEH with the metal site replaced with copper and indium, respectively. Copper and indium are metal elements with the highest and the lowest LJ energy parameter among all metal elements considered in this work. The difference in the minimum energy between $^{12}CH_4$ and $^{13}CH_4$ is similar for RUBLEH with different metal sites. However, along the minimum energy pathway (MEP), RUBLEH with indium has a much lower energy profile and the energy barrier, which explains the increase of permeability with the increase of energy parameter of the metal site. Reducing the LJ energy parameter for the metal site raises the minimum energy profile but lowers the absolute value of the energy barrier. Because $^{12}CH_4$ and $^{13}CH_4$ have similar minimum energy profiles, the smaller the

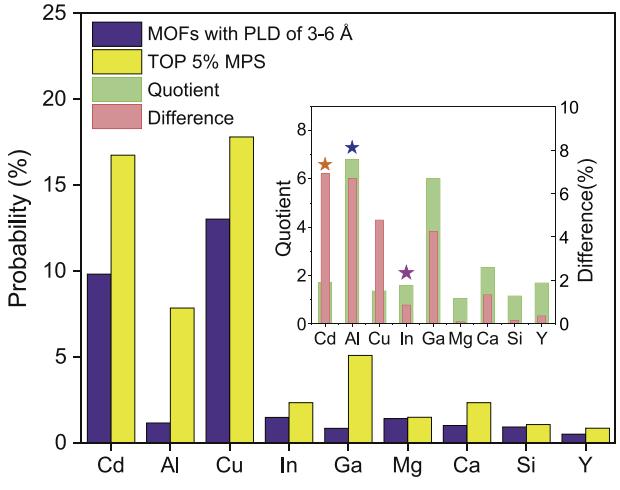

Fig. 6. Distributions of the metal elements (ratio more than 0.1% in database) in MOFs with a significant higher distribution in top 5% membrane performance score. Blue, orange and pink stars denote the metal elements with the largest quotient, the largest difference in MPS, and the largest energy parameter.

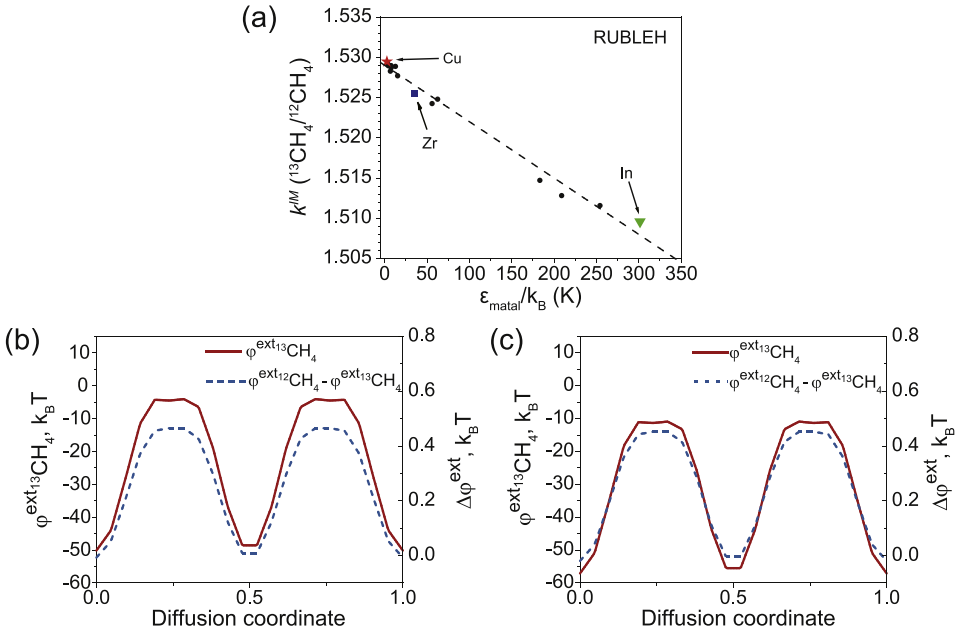

Fig. 7. (a) Ideal membrane selectivity versus the energy parameter of different metal elements for modification of RUBLEH. Minimum energy along the diffusion coordinate of methane with the RUBLEH metal site replaced by copper (b) and by indium (c).

absolute value of the energy barrier, the more difference in the permeability of the isotopic forms of methane, leading to a higher membrane selectivity.

For top 5 MOFs with the highest MPS, we consider aluminum and cadmium as a substitute to the original metal sites because their percentages in MOFs with top 5% MPS are much higher than the background values in comparison with the other metal elements. Indium is also considered for the substitution of the metal sites as it has the largest LJ energy parameter. Table S8 lists the permeability, membrane selectivity, and MPS of the top 5 MOFs with their original and modified metal sites.

Table 4 summarizes the performance of MOFs with the highest MPS after modifications of their metal sites. For all cases, the MPS values of the modified MOFs are always higher than those corresponding to the original MOFs. The performance of MOFs with their original metal sites is also listed for comparison. The improvement in MPS can be attributed to both the increase of permeability and the increase of selectivity. Interestingly, an increase of the energy parameter of metal sites leads to both a higher permeability and a better membrane selectivity. MOFs with high MPS values for separating $^{12}CH_4/^{13}CH_4$ are mainly contributed to high permeability and intermediate membrane selectivity, implying that the MEP is mostly attractive. As a result, metal sites with a higher energy parameter can better distinguish the isotopic molecules. Besides, they can reduce the energy along the diffusion path because metal sites mainly contribute an attractive energy to the energy barrier. It is worth noting that, for all top performance MOFs, the highest MPS is realized by replacing the original metal site with In, implying that metal elements with higher LJ energy parameters would be a good choice for the replacement of the MOF metal site for the better separation of isotopic components.

4. Conclusions

In this work, we have explored the potential application of nanoporous materials both as absorbents and as membranes for separation of carbon isotopes ($^{12}CH_4/^{13}CH_4$) by screening

Table 4
Performance of the top 5 ranked MOFs after substitution of the metal sites.

MOF	Metal site		P ($^{12}CH_4$) (barrer)	k^{IM} ($^{13}CH_4/^{12}CH_4$)	MPS
	Original	Modified			
ERANAO	Zr		5.103×10^{15}	1.0553	5.683×10^{15}
		In	2.610×10^{18}	1.0433	2.841×10^{18}
XOPVOO	Ni		3.494×10^{14}	0.9561	3.655×10^{14}
		In	6.721×10^{14}	0.9536	7.048×10^{14}
OQIKOQ	Zr		1.276×10^{14}	0.9141	1.396×10^{14}
		In	2.585×10^{14}	0.9133	2.830×10^{14}
OJUNIS	Zn		1.510×10^{13}	0.9264	1.630×10^{13}
		In	2.734×10^{13}	0.9246	2.956×10^{13}
WOMFEK	Mn		1.466×10^{12}	0.9591	1.528×10^{12}
		In	1.480×10^{13}	0.9534	1.553×10^{13}

the ideal selectivity and capacity of 12,478 computation-ready, experimental (CoRE) MOF structures. While these materials are commonly regarded as good adsorbents, a higher separation efficiency may be accomplished by using them as membranes for $^{12}CH_4/^{13}CH_4$ separation because a good balance between the separation selectivity and capacity can be achieved. Among all MOFs in the CoRE database, we find that RUBLEH exhibits the highest membrane selectivity for the separation of $^{12}CH_4/^{13}CH_4$ at room temperature, which can reach up to 1.530 with the substitution of Zr in the original structure with Cu. For comparison, the relative volatility of these isotopic forms of methane is less than 1.01 even at 100 K and a similar value was observed for the selectivity according to chromatography measurement. Therefore, MOF membranes can be much more efficient than conventional methods for isotope separations. Most importantly, the nanoporous materials enable isotope separation at ambient conditions thereby greatly saving the equipment and operation costs.

We have also analyzed the structural features and metal sites of those MOFs with top membrane selectivity (k^{IM}) and top membrane performance scores (MPS). For MOFs with top 5% membrane selectivity, the PLD is close to the LJ diameter of the isotopic methane thereby providing good sieve effects on $^{12}CH_4$ and $^{13}CH_4$. For MOFs with top 5% membrane selectivity, the LCD is distributed between 3 and 5 Å while the optimal void fraction is around 0.4. These structural features define an optimized diffusion path to distinguish gas molecules hopping between neighboring pores. The metal elements in those promising MOFs have LJ energy parameters (ε/k_B) spanning from 2.52 to 301.43 K. However, the percentages of metal elements with a high energy parameter exceeds the background values more significantly in terms of both quotient and difference calculated from the percentages of metal sites in promising MOFs divided and subtracted by that in the background, respectively. In order to achieve a high MPS, the membrane selectivity is slightly comprised for the permeability as it is easier to improve permeability than the selectivity for the separation of $^{12}CH_4/^{13}CH_4$. As a result, MOFs with top 5% MPS exhibit structural features that make the gas molecules less confined than those with top 5% membrane selectivity. Similarly, metal elements with high energy parameters have a significantly high probability of presence in the promising MOFs ranked according to MPS in comparison with the background distribution.

We have further investigated how modification of metals sites would affect the performance of MOFs for $^{12}CH_4/^{13}CH_4$ separation. The selectivity decreases with the increase of the energy parameter of the metal site owing to a stronger attraction with the gas molecules. Besides, a metal site with a larger energy parameter would lower the energy barrier for gas diffusion because it mainly contributes an attractive energy to the gas-substrate interactions. On the other hand, different metal sites give almost the same relative energy difference along the minimum energy pathway for the isotopic pairs of methane. For MOF with high MPS, the MPS is improved by changing the original metal sites with ones with higher energy parameters. Since a higher value of MPS implies higher permeability and larger membrane selectivity, we conjecture that metal sites with a higher binding energy can further improve the permeability and selectivity for better $^{12}CH_4/^{13}CH_4$ separation. As all materials considered in this work have been synthesized, the theoretical predictions can be directly testable with experiments. The efficient separation of isotopic systems enabled by nanoporous membranes may have drastic implications in the broad applications of stable carbon isotopes for chemical and biological analysis, in early diagnosis of human diseases, and in determining chemical reaction mechanisms.

Conflict of interest

The authors claim no potential conflict of interest including any financial, personal or other relationships with other people or organizations within three years of beginning the submitted work that could inappropriately influence, or be perceived to influence their work.

Acknowledgement

This work is financially supported by the National Science Foundation Harnessing the Data Revolution Big Idea under Grant No. NSF 1940118. This work is also supported by the State Key Laboratory of Chemical Engineering (SKL-CHE-20).

Appendix A. Supplementary data

Supplementary data to this article can be found online at https://doi.org/10.1016/j.gee.2020.07.025.

References

[1] M. Matucha, W. Jockisch, P. Verner, G. Anders, J. Chromatogr. A 588 (1991) 251–258.
[2] R.A. de Vries, M. de Bruin, J.J.M. Marx, A. van de Wiel, Nucl. Med. Biol. 20 (1993) 809–817.
[3] P. Ciais, P.P. Tans, M. Trolier, J.W. White, R.J. Francey, Science 269 (1995) 1098–1102.
[4] E.D. Oziashvili, A.S. Egiazarov, Russ. Chem. Rev. 58 (1989) 325–336.
[5] H.O. Meyer, G.L. Moake, P.P. Singh, Phys. Rev. C 23 (1981) 616–622.
[6] K. Takeshita, Y. Nakano, M. Shimizu, Y. Fujii, J. Nucl. Sci. Technol. 39 (2002) 1207–1212.
[7] Y. Tian, W.Y. Fei, J.Z. Wu, Ind. Eng. Chem. Res. 57 (2018) 5151–5160.
[8] M. Zhou, Y. Tian, W. Fei, J. Wu, J. Phys. Chem. C 123 (2019) 7397–7407.
[9] M. Zhou, A. Vassallo, J. Wu, J. Membr. Sci. 598 (2020) 117675.
[10] J.I.F. Slaets, C. Resch, L. Mayr, G. Weltin, M. Heiling, R. Gruber, G. Dercon, Rapid Commun. Mass Spectrom. 34 (2020) e8669.
[11] H. Oh, M. Hirscher, Eur. J. Inorg. Chem. 2016 (2016) 4278–4289.
[12] F. Bruner, G.P. Cartoni, M. Possanzini, Anal. Chem. 41 (2002) 1122–1124.
[13] G. Berger, C. Prenant, J. Sastre, D. Comar, Appl. Radiat. Isot. 34 (1983) 1525–1530.
[14] F. Bruner, G.P. Cartoni, A. Liberti, Anal. Chem. 38 (1966) 298–303.
[15] R.C. Jones, W.H. Furry, Rev. Mod. Phys. 18 (1946) 151–224.
[16] B.B. Mcinteer, Separ. Sci. Technol. 15 (2006) 491–508.

[17] H.L. Li, Y.L. Ju, L.J. Li, D.G. Xu, Chem. Eng. Process 49 (2010) 255–261.
[18] E.H. Dulf, C.-I. Pop, F. Dulf, Separ. Sci. Technol. 47 (2012) 1234–1240.
[19] D.C. Dumitrache, B.D. Schutter, A. Huesman, E. Dulf, J. Process Contr. 22 (2012) 798–808.
[20] J.Y. Kim, R. Balderas-Xicohtencatl, L. Zhang, S.G. Kang, M. Hirscher, H. Oh, H.R. Moon, J. Am. Chem. Soc. 139 (2017) 15135–15141.
[21] M. Mu, J. Cheng, C. Dai, N. Liu, Z. Lei, Y. Ding, J. Lu, Green Energy Environ. 4 (2019) 190–197.
[22] S. Ren, Y. Hou, K. Zhang, W. Wu, Green Energy Environ. 3 (2018) 179–190.
[23] T.R. Mazur, B. Klappauf, M.G. Raizen, Nat. Phys. 10 (2014) 601–605.
[24] K.J. Nihill, J.D. Graham, S.J. Sibener, Phys. Rev. Lett. 119 (2017) 176001.
[25] M. Dong, X. Mao, J.J. Gonzalez, J. Lu, R.E. Russo, Anal. Chem. 85 (2013) 2899–2906.
[26] M. Kumar, V. Gupta, A.K. Nath, Appl. Phys. B 80 (2005) 757–763.
[27] C. Chen, X. Feng, Q. Zhu, R. Dong, R. Yang, Y. Cheng, C. He, Inorg. Chem. 58 (2019) 2717–2728.
[28] H. Yuan, J. Chen, D. Li, H. Chen, Y. Chen, Chem. Eng. J. 373 (2019) 171–178.
[29] C. Miao, J. Mol. Struct. 1193 (2019) 286–293.
[30] Y. Wang, T. Du, H. Jia, Z. Qiu, Y. Song, Solid State Sci. 97 (2019) 105985.
[31] L. Wang, J. Inorg. Organomet. Polym. Mater. 30 (2019) 291–298.
[32] Y.G. Chung, J. Camp, M. Haranczyk, B.J. Sikora, W. Bury, V. Krungleviciute, T. Yildirim, O.K. Farha, D.S. Sholl, R.Q. Snurr, Chem. Mater. 26 (2014) 6185–6192.
[33] Y.G. Chung, E. Haldoupis, B.J. Bucior, M. Haranczyk, S. Lee, H. Zhang, K.D. Vogiatzis, M. Milisavljevic, S. Ling, J.S. Camp, B. Slater, J.I. Siepmann, D.S. Sholl, R.Q. Snurr, J. Chem. Eng. Data 64 (2019) 5985–5998.
[34] B. Wang, L.H. Xie, X. Wang, X.M. Liu, J. Li, J.R. Li, Green Energy Environ. 3 (2018) 191–228.
[35] H. Oh, I. Savchenko, A. Mavrandonakis, T. Heine, M. Hirscher, ACS Nano 8 (2014) 761–770.
[36] H. Thakkar, S. Eastman, Q. Al-Naddaf, A.A. Rownaghi, F. Rezaei, ACS Appl. Mater. Interfaces 9 (2017) 35908–35916.
[37] K. Lee, J.D. Howe, L.C. Lin, B. Smit, J.B. Neaton, Chem. Mater. 27 (2015) 668–678.
[38] L. Zhu, X.Q. Liu, H.L. Jiang, L.B. Sun, Chem. Rev. 117 (2017) 8129–8176.
[39] M. Tong, Y. Lan, Q. Yang, C. Zhong, Green Energy Environ. 3 (2018) 107–119.
[40] P. Horcajada, R. Gref, T. Baati, P.K. Allan, G. Maurin, P. Couvreur, G. Ferey, R.E. Morris, C. Serre, Chem. Rev. 112 (2012) 1232–1268.
[41] J. Teufel, H. Oh, M. Hirscher, M. Wahiduzzaman, L. Zhechkov, A. Kuc, T. Heine, D. Denysenko, D. Volkmer, Adv. Mater. 25 (2013) 635–639.
[42] H. Oh, K.S. Park, S.B. Kalidindi, R.A. Fischer, M. Hirscher, J. Mater. Chem. A 1 (2013) 3244–3248.
[43] L.E. Kreno, K. Leong, O.K. Farha, M. Allendorf, R.P. van Duyne, J.T. Hupp, Chem. Rev. 112 (2012) 1105–1125.
[44] J.Y. Kim, H. Oh, H.R. Moon, Adv. Mater. 31 (2019) 1805293.
[45] A.K. Rappe, C.J. Casewit, K.S. Colwell, W.A. Goddard, W.M. Skiff, J. Am. Chem. Soc. 114 (1992) 10024–10035.
[46] J. Bigeleisen, C.B. Cragg, M. Jeevanandam, J. Chem. Phys. 47 (1967) 4335–4346.
[47] W.A. van Hook, L.P.N. Rebelo, M. Wolfsberg, J. Phys. Chem. 105 (2001) 9284–9297.
[48] U. Setzmann, W. Wagner, J. Phys. Chem. Ref. Data 20 (1991) 1061–1155.
[49] A. Lotfi, J. Vrabec, J. Fischer, Mol. Phys. 76 (1992) 1319–1333.
[50] A.L. Myers, J.M. Prausnitz, AlChE J. 11 (1965) 121–127.
[51] S. Keskin, D.S. Sholl, Langmuir 25 (2009) 11786–11795.
[52] E. Haldoupis, S. Nair, D.S. Sholl, J. Am. Chem. Soc. 132 (2010) 7528–7539.
[53] Y. Tian, X. Xu, J. Wu, Langmuir 33 (2017) 11797–11803.
[54] W. E, W. Ren, E. Vanden-Eijnden, J. Chem. Phys. 126 (2007) 164103.
[55] T.F. Willems, C.H. Rycroft, M. Kazi, J.C. Meza, M. Haranczyk, Microporous Mesoporous Mater. 149 (2012) 134–141.
[56] W.K. Kim, M. Kanduc, R. Roa, J. Dzubiella, Phys. Rev. Lett. 122 (2019) 108001.
[57] M. Agrawal, R. Han, D. Herath, D.S. Sholl, Proc. Natl. Acad. Sci. Unit. States Am. 117 (2020) 877–882.